Microelectronic Engineering 152 (2016) 41–47

Contents lists available at ScienceDirect

Microelectronic Engineering

journal homepage: www.elsevier.com/locate/mee

# The effects of post-deposition ion-beam bombardment with oxygen on the Co surface in modifying the magnetic properties of Co thin films

X. Li [a], K.-W. Lin [b,*], H.-T. Liang [b], P.-L. Liu [c,d], W.-C. Lo [b], D.L. Cortie [e], F. Klose [f], J. van Lierop [g,*], L. Li [a], Philip W.T. Pong [a,*]

[a] Department of Electrical and Electronic Engineering, The University of Hong Kong, Hong Kong
[b] Department of Materials Science and Engineering, National Chung Hsing University, Taichung 402, Taiwan
[c] Graduate Institute of Precision Engineering, National Chung Hsing University, Taichung 402, Taiwan
[d] Department of Physics, Norwegian University of Science and Technology, N-7491 Trondheim, Norway
[e] Quantum Matter Institute, Department of Physics and Astronomy, University of British Columbia, Vancouver, BC V6T1Z4, Canada
[f] Australian Nuclear Science and Technology Organisation, NSW 2234, Australia
[g] Department of Physics and Astronomy, University of Manitoba, Winnipeg, MB R3T 2N2, Canada

ARTICLE INFO

*Article history:*
Received 17 July 2015
Received in revised form 18 December 2015
Accepted 28 December 2015
Available online 30 December 2015

*Keywords:*
Cobalt
Ion-beam bombardment
Magnetic property

ABSTRACT

Ion beam bombardment is a useful surface modification method in tailoring the microstructure and magnetic properties of ferromagnetic thin films. In this paper, Co thin films were bombarded by $Ar^+$ ion beam with oxygen and then capped with Al (to prevent oxidation). The oxygen content was altered from 0 to 41% to investigate the ion-beam bombardment effect. An oxide layer containing $Al_2O_3$, $Co_3O_4$ and CoO was formed after the ion-beam bombardment with oxygen, as characterized by x-ray photoelectron spectroscopy, high-resolution transmission electron microscopy, selected area electron diffraction, and x-ray diffraction. Enhanced coercivities ($H_c$'s) (from 4.14 kA/m to 7.96 kA/m) and loop squareness ($M_r/M_s$, from 0.5 to 0.8) was induced by pure $Ar^+$ ion-beam bombardment that resulted in domain wall pinning due to bombardment-induced defects and Co spin reordering. $H_c$ exhibited a strong dependence on the oxygen content in the ion beam, due to the nature of the cobalt oxide formation. Field cooling to 180 K resulted in increased squareness ($M_r/M_s = 0.9$) and reduced $H_c$. The low-field magnetization measured during zero field and field cooling to further investigate the exchange bias magnetism identified an irreversibility temperature at 320 K in a film treated by ion-beam bombardment with an $O_2$/Ar ratio of 21%.



## 1. Introduction

Controlling and modifying the magnetic properties of ferromagnetic (FM) thin films have been drawing significant research interest for tailoring the performance of spintronic devices such as giant magnetoresistance sensors [1] and magnetic random access memories [2]. The magnetic properties of ferromagnetic (FM) thin films could be tailored by conducting surface modification or post treatment. Ion-beam bombardment is a frequently used surface modification technique — ion-beam bombardment can modify the orientation of FM spins, resulting in altered coercivity ($H_c$) and exchange bias ($H_{ex}$) [3]. Also, the chemical composition of the FM layer can also be changed by introducing a reactive gas (such as oxygen) into the ion beam [4]. The formed compounds and the FM layer will establish interactions (such as exchange coupling [5]) and modify the magnetic properties. Post treatment is another effective method for altering both the microstructure and magnetic properties of magnetic thin films. Field cooling (FC) and zero-field cooling (ZFC) is used to change the magnetic properties of FM thin films. The orientations of FM spins are frozen when cooling through the Curié temperature ($T_C$), maintaining the state favored by the internal magnetic anisotropy energy (ZFC) or the external Zeeman energy (FC) [6]. Thus the orientations of FM spins are influenced strongly by the cooling field.

Cobalt is a ferromagnetic material with high $T_C$ (~1388 K [7]) and large anisotropy energy ($4.26 \times 10^6$ erg/cm$^3$ for α-Co [8]), thus having broad applications in magnetic recording [9] and magnetic multilayers with perpendicular magnetic anisotropy [10,11]. Certain cobalt oxides are antiferromagnetic at low temperatures, such as CoO ($T_N$ ~ 291 K [12]) and $Co_3O_4$ ($T_N$ ~ 40 K [13]). Ever since the discovery of the exchange bias effect in CoO coated Co particles [14], various surface modification techniques have been introduced to alter the magnetic properties of Co thin films. The CoO could be formed as a result of natural oxidation in air or oxygen [15–17], in-situ oxidation during Co deposition [18–22], and oxygen ion implantation [23,24]. Ion-beam bombardment was also reported in modifying the magnetic properties of Co thin films. In-situ Ar-ion-beam bombardment with oxygen during

* Corresponding authors.
*E-mail addresses:* kwlin@dragon.nchu.edu.tw (K.-W. Lin), johan@physics.umanitoba.ca (J. van Lierop), ppong@eee.hku.hk (P.W.T. Pong).

http://dx.doi.org/10.1016/j.mee.2015.12.019
0167-9317/

Co deposition resulted in pillar like CoO structures in the Co layer [25]. However, the effect of post ion-beam bombardment after the Co deposition on modifying the microstructure and magnetic properties of Co thin film remained unclear, and the influence of oxygen content in the ion beam was not yet investigated. In this paper, the composition, microstructure, and magnetic properties of a Co layer treated by post ion-beam bombardment with oxygen was investigated. The changes in the structural and magnetic properties induced by ion-beam bombardment were tracked by changing the oxygen content in the ion beam from 0% to 41%. The comparison between field-cooling (FC) and zero-field-cooling (ZFC) the film for magnetization measurements further revealed the applied field effect in the Co-O/Co structures' magnetism.

## 2. Experimental methods

26-nm-thick Co single layers were deposited on thermally oxidized silicon substrates by dual-ion-beam deposition technique [26]. A Kaufman deposition source operated at $V_K = 800$ V was engaged to sputter the Co target at base pressure of $4.0 \times 10^{-7}$ Torr and working pressure of $3.0 \times 10^{-4}$ Torr. After the Co deposition, $Ar^+$ ion-beam bombardment with oxygen ($O_2$/Ar ratio ranging from 0 to 41%) was conducted on Co surface for 10 min by an End hall ion source operated at $V_{EH} = 70$ V. 6-nm-thick Al layers were deposited subsequently to prevent surface oxidation.

The composition and binding energies of the Al 2p, Co 2p and O 1s transitions of the Al/Co–O (15% $O_2$/Ar)/Co and Al/Co–O (41% $O_2$/Ar)/Co films were characterized by a commercial ULVAC-PHI (PHI 5000 Versa Probe) x-ray photoelectron spectroscopy (XPS) equipped with a X-ray source (Al Kα radiation) and a 5 kV Ar ion gun. The surface and cross-sectional morphologies of both ion-beam bombarded and un-bombarded Co layers were characterized by a JOEL-2100F high-resolution transmission electron microscope (HRTEM). The crystalline structures were characterized from selected area electron diffraction (SAED) by HRTEM and x-ray diffraction (XRD) patterns by a Bruker-AXS D8 Advance. The magnetic hysteresis loops of all the samples were measured by an ADE-DMS 1660 vibrating sample magnetometer (VSM) at room temperature and 180 K after cooling in a 1.2 T magnetic field. The temperature dependent magnetization was measured with 10 mT between 50 K and 400 K by a Quantum Design VSM after FC and ZFC processes.

## 3. Results and discussions

The depth profile XPS of Al/Co–O (15% $O_2$/Ar)/Co and Al/Co–O (41% $O_2$/Ar)/Co films are shown in Fig. 1 and Fig. 2, respectively. The samples were sputter etched at ~13.3 nm/min, and the bonding energy spectra and concentrations of Co, Al, O and Si were characterized at 0.1 min or 0.08 min intervals. In the depth profile of the elemental concentration in the Al/Co–O (15% $O_2$/Ar)/Co film (Fig. 1(a)), a clear oxide layer (corresponding to sputtering time ($T_{sp}$) ranging from 0.4 min to 0.8 min) is shown. In addition, the high concentration of Al in the oxide layer (30%) evidences strong Al diffusion. Both metallic Al and alumina exist at the Al/oxide interface, as shown in the double peak at 72.2 eV and 74.6 eV in the Al 2p spectrum (Fig. 1 (b), $T_{sp} = 0.4$ min). Al atoms in the form of $Al_2O_3$ and a $CoAl_x$ alloy were detected at the oxide/Co interface, which is indicated by the broadened Al 2p peak at around 74.8 eV (Fig. 1 (b), $T_{sp} = 0.7$ min). The Al atoms in the Co layer are likely due to the Al diffusion. Another phase at the oxide/Co interface is cobalt oxide, as shown by the sub-peak at 780.3 eV ($Co_3O_4$) [27] and 780.9 eV (CoO) [28] in Co $2p_{3/2}$ spectra (Fig. 1 (c), $T_{sp} = 0.7$ min). The formation of a $CoAl_x$ alloy was also indicated by

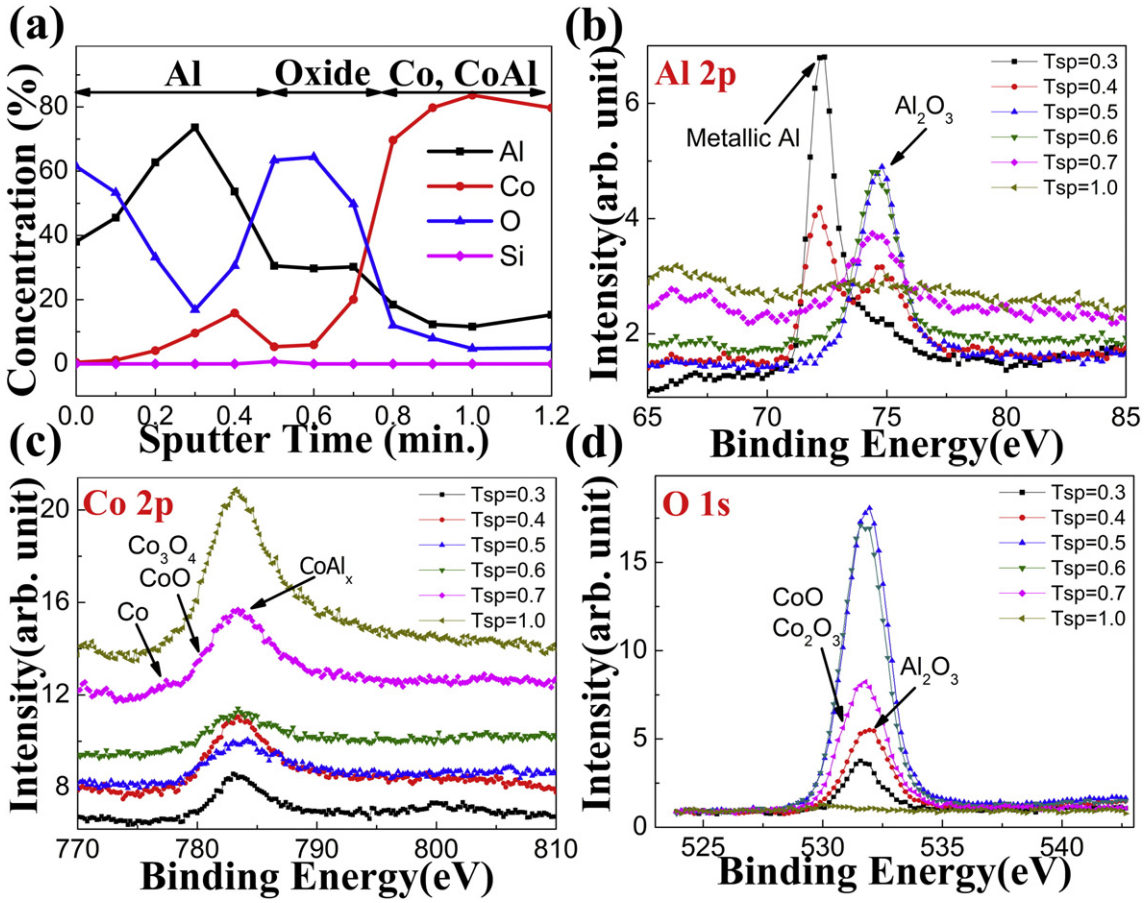


**Fig. 1.** (a) The depth profile of the chemical concentrations in the Al/Co–O (15% $O_2$/Ar)/Co and (b) the Al 2p, (c) Co 2p, and (d) O 1s spectra at each sputter etching time measured by XPS.

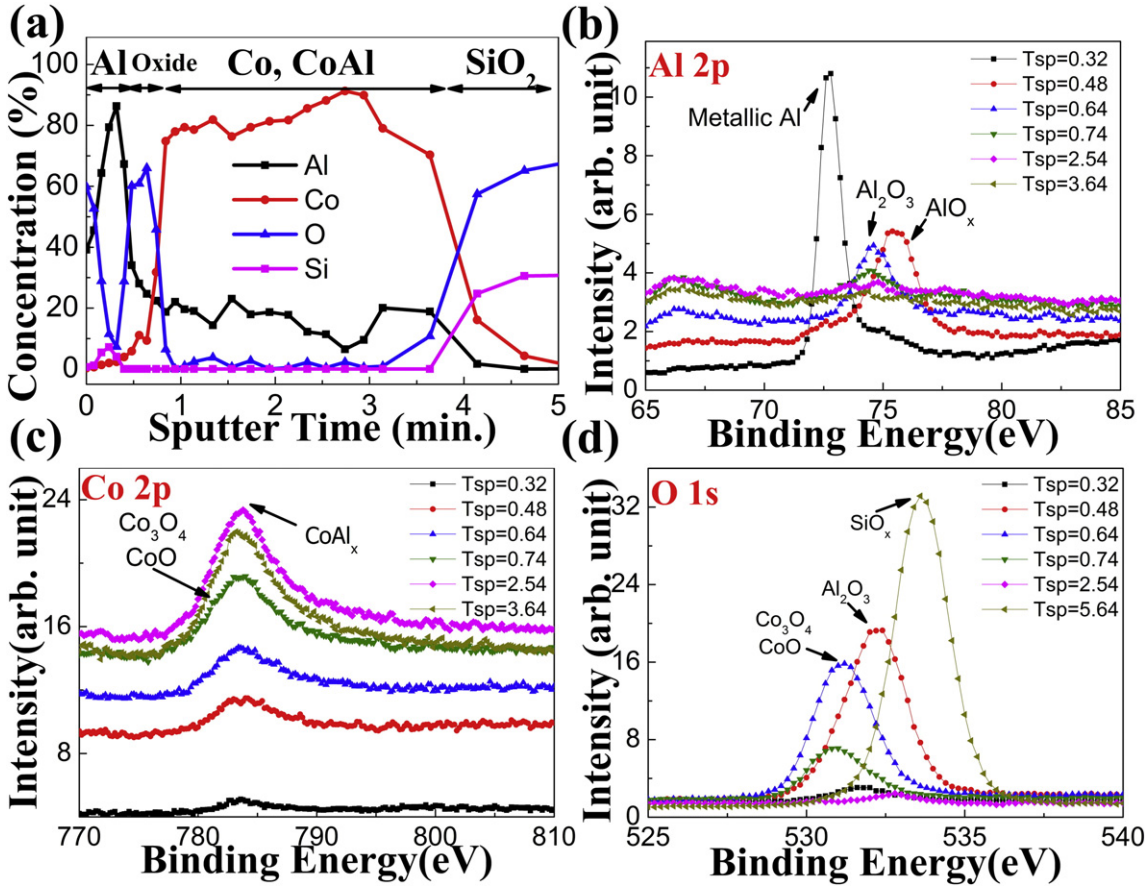


**Fig. 2.** (a) The depth profile of the chemical concentrations in Al/Co–O (41% $O_2$/Ar)/Co and (b) the Al 2p, (c) Co 2p, and (d) O 1s spectra at each sputter etching time measured by XPS.

the major peak at 783 eV in Fig. 1 (c). The O 1s peak at around 531.5 eV indicates that the major oxide in the oxide layer is $Al_2O_3$. However, the asymmetric O 1s peak at $t_{sp.} = 0.7$ min contains a sub-peak at 531 eV, which corresponds to the binding energy of Co–O in $Co_3O_4$ [29]. The chemical composition of the Al/Co–O (41% $O_2$/Ar)/Co (Fig. 2 (a)) is similar to that in the Al/Co–O (15% $O_2$/Ar)/Co. However, the increased oxygen content in the ion beam used during deposition resulted in more oxidation of Al and Co. A new Al 2p peak at 75.4 eV in the Al/oxide interface was observed in Fig. 2 (b) ($t_{sp} = 0.48$ min), indicating the changes in stoichiometry of $AlO_x$. In addition, the formation of cobalt oxides was greatly promoted in the oxide/Co interface. The asymmetric Co 2p peak at the oxide layer contains a sub-peak at around 781 eV (Fig. 2 (c), $t_{sp.} = 0.74$ min), which possibly derived from the Co–O band in $Co_3O_4$ (780.3 eV [27]) and in CoO (780.9 eV [28]). The peak shifting from 532 eV (Fig. 2 (d), $T_{sp} = 0.48$ min) to 531 eV (Fig. 2 (d), $T_{sp} = 0.64$ min and 0.74 min) also indicates the composition transition from the Al/oxide interface to the oxide/Co interface is $Al_2O_3$ to CoO/$Co_3O_4$. It should be noted that the concentration of Al (~20%) in the Co layer of the Al/Co–O (41% $O_2$/Ar)/Co film is slightly greater than that of the Al/Co–O (15% $O_2$/Ar)/Co film (10%–15%). It is possible that the measured Al content is partially contributed by the mixing during sputter etching. However, since the same sputtering condition was used during the characterization of the two samples, the contribution of the mixing should be the same. So Al diffusion was more pronounced in the Co layers bombarded under higher $O_2$/Ar ratio, which was interpreted as follows. The higher $O_2$/Ar ratio resulted in more oxides on the surface of Co, as relatively higher O content was observed in the oxide layer of Al/Co–O (41% $O_2$/Ar)/Co (67% in Fig. 2 (a)) than that in Al/Co–O (15% $O_2$/Ar)/Co (63% in Fig. 1(a)). The grain boundaries and dislocations between the oxides and adjacent phases provided diffusion path for the subsequently deposited Al atoms. So the higher content of oxides at higher $O_2$/Ar ratio resulted in stronger Al diffusion into Co layer.

In order to investigate the effect of ion-beam bombardment on the crystalline structure, the cross-sectional morphology of the Al/Co–O (30% $O_2$/Ar)/Co film was characterized by HRTEM, as shown in Fig. 3. Unlike the in-situ bombarded Co/CoO bilayer, which generated spike-like CoO structures penetrating into Co [30], the post-bombardment only resulted in a 4-nm-thick disordered oxide layer on the surface of Co. This is because the relatively low kinetic energy of $O_2^-$ ions (70 eV) resulted in small penetration depth inside Co. To compare the interplanar lattice spacing of the crystalline structures depicted in Fig. 3, a face-centered cubic (FCC) Co (space group: 225 *fm-3m*), hexagonal close-packed (HCP) Co (space group: 194 *P63-mmc*), rocksalt CoO (space group: 225 *fm-3m*), and spinel $Co_3O_4$ (space group: 227 *Fd-3m*) lattices were investigated by conducting first-principles density functional theory (DFT) calculations. We employed the Cambridge Serial Total Energy Package (CASTEP) [31] based on spin polarized GGA-PW91 functionals [32,33]. The interlayer spacings in regions (1) and (2) of Fig. 3 are 2.05 Å and 2.08 Å, respectively, in excellent agreement with the corresponding calculated values, 2.05 Å, determined from the interplanar spacing of the (111) plane in the FCC Co. The interlayer spacings in regions (3) and (4) of Fig. 3 are 2.12 Å and 2.11 Å, respectively, which are approximately 3% smaller than the calculated values of 2.18 Å, determined from the interplanar spacing of the (100) plane in the HCP Co. This smaller interlayer spacing is possibly due to the lattice mismatch with the adjacent heterogeneous phases. In region (5) of the oxide layer of Fig. 3, the interlayer spacing is 2.13 Å, which closely matches the value 2.14 Å found for the interplanar spacing of the (200) plane in rocksalt CoO. On the other hand, we find that the interlayer spacing in region (6) of the oxide layer of Fig. 3 is 2.43 Å, which is in good agreement with the value of 2.47 Å calculated from the

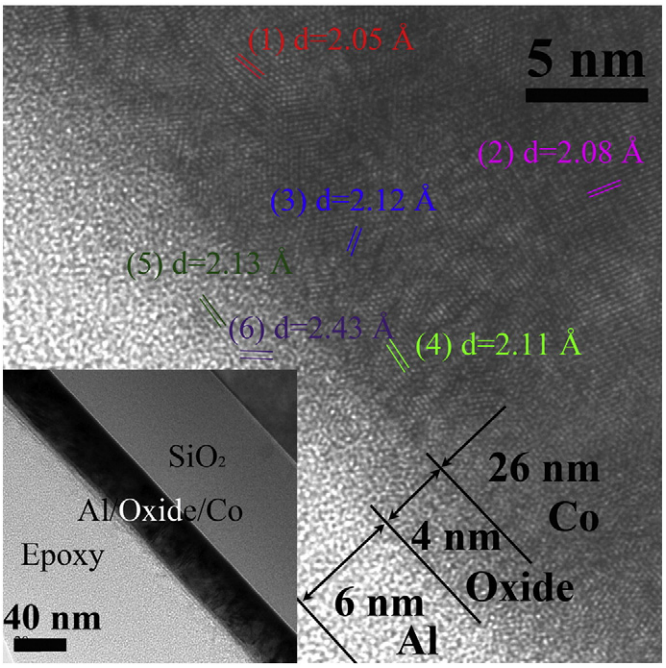


**Fig. 3.** The cross-sectional morphology of the Al/Co–O (30% $O_2$/Ar)/Co film characterized by HRTEM.

interplanar spacing of the (311) plane in the spinel $Co_3O_4$. It should be noted that bombardment-induced Co-oxide grains are not likely to be the highly ordered structures since they are small in size and are surrounded by amorphous phases. This may result in deviations in lattice parameters and magnetic properties from the ordered crystalline phases.

In addition, the morphologies of all the samples were characterized by bright field image HRTEM, and the crystalline structures were analyzed from their SAED patterns, shown in Fig. 4. The Al single layer exhibited amorphous structures in the films, as shown by the extended SAED rings in the inset of Fig. 4(a). The un-bombarded Al/Co bilayers, on the other hand, possessed polycrystalline structures with grain sizes ranging from 5 nm to 15 nm (Fig. 4(b)). (002) plane of HCP Co can be observed in the electron diffraction rings in the inset of Fig. 4(b). CoAl alloy was observed in the un-bombarded Al/Co bilayers, shown by the innermost SAED ring, which corresponds to the (100) and (111) planes in B2 CoAl. The ion-beam bombardment altered the grain sizes, crystalline phases, and preferred orientations of the bilayers, resulting in large changes in surface morphologies as shown in Fig. 4(c) to (h). Broadened distributions of grain sizes, and nonuniform surface textures were observed on the surface of the ion-beam bombarded samples. The pure $Ar^+$ ion beam changed the preferred orientation of the grains in Co layer, as shown by the electron diffraction rings corresponding to HCP Co (100), (102) and (112) planes in the inset of Fig. 4(c). The CoAl (210) plane was observed in all the ion-beam bombarded films. The preferred orientations of the spinel $Co_3O_4$ phase formed by the ion-beam bombardment with oxygen was (511) (insets of Fig. 4(d) to (h)). This is also different from that of the naturally oxidized $Co_3O_4$ (311). The samples bombarded by the ion beam with oxygen also exhibited the rock-salt CoO phase as shown by the CoO (331) and (111) electron diffraction ring in the insets of Fig. 4(d) to (h).

The changes in crystalline structure among films were also observed in their respective XRD patterns, presented in Fig. 5. A broadened major reflection at $2\theta = 44.3°$ was observed in the XRD patterns of all the samples. This broadened reflection resulted from the overlay of ordered B2 CoAl (110) ($2\theta = 44.741°$), and HCP Co (002) ($2\theta = 44.762°$) reflections. Co atoms form HCP Co ($a = 2.507$ Å, $c = 4.07$ Å) and B2 CoAl ($a \sim 2.83$ Å) lattices in the ion-beam bombarded Co layers, as observed

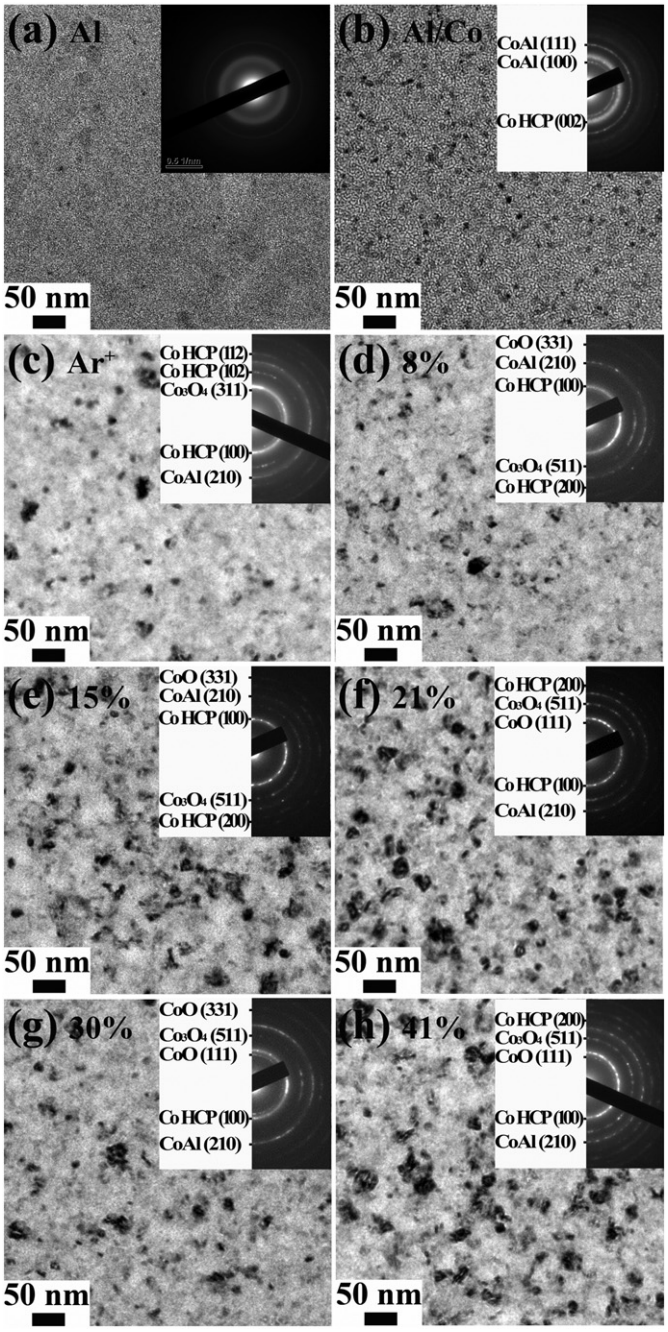


**Fig. 4.** The morphologies and SAED patterns of the un-bombarded and ion-beam bombarded Co with Al capping layer characterized by TEM.

in the SAED patterns (Fig. 4) and XPS spectrum (Fig. 1 and Fig. 2). In addition, rock-salt CoO ($a \sim 4.24$ Å) and spinel $Co_3O_4$ ($a \sim 8.09$ Å) was formed as a result of the oxidization of $O_2$/Ar ion beam, as proved by the CoO (200) peak at $2\theta = 42.6°$ and $Co_3O_4$ (222) peak at $2\theta = 38.6°$ in the XRD pattern.

The compounds that formed at the interface can be interpreted by way of the thermodynamics point of view. During the ion-beam bombardment with oxygen, cobalt oxides including CoO and $Co_3O_4$ could be formed. However, in the initial stage of the bombardment, oxygen atoms preferred to form $Co_3O_4$ since $Co_3O_4$ (−891 KJ/mol [34]) has more negative enthalpy of formation than CoO (−237.9 KJ/mol [34]). As the amount of oxygen on the Co surface increases, CoO content could also be formed although the content is relatively low. This is proved by the XPS results which indicate that the content of cobalt

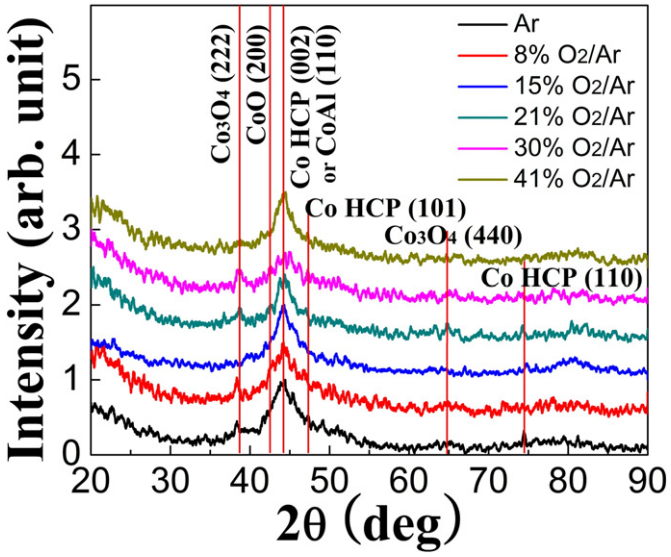


**Fig. 5.** The XRD pattern of the Co layers bombarded by ion beam with $O_2$/Ar ratio ranging from 0 to 41% and capped with Al layer.

oxides increased remarkably in samples bombarded by the ion beam with higher $O_2$/Ar ratio. The abundant oxygen atom at the surface of the Co layer reacted with the subsequently deposited Al since $Al_2O_3$ has the most negative enthalpy of formation (−1669.8 KJ/mol [34]). Since no evidence of $Al_2O_3$ grains was observed in the SAED and XRD analyses, the alumina more likely possesses an amorphous structure. Despite its small enthalpy of formation (−110 kJ/mol [35]), CoAl was also formed at the Al/Co interface where both Co and Al were in supersaturated state [35], as shown in the XRD patterns. The above analyses in chemical compositions and crystalline structures reveal that the chemical contents and microstructures were altered by the ion-beam bombardment. These changes influenced their magnetic properties to a great extent, which were characterized by VSM measurements.

The magnetic hysteresis loops measured at 298 K and 180 K after field cooling with 1.2 T magnetic field are shown in Fig. 6(a) and (b). At 298 K, the un-bombarded Co layer presented soft magnetism (low $H_c$ of 4.14 kA/m) with a concomitant rounded hysteresis loop ($M_r/M_{s.}$ = 0.5). The pure $Ar^+$ ion-beam bombardment resulted in enhanced $H_c$ (7.96 kA/m) and squareness ($M_r/M_{s.}$ = 0.8). This is likely due to the formation of defects (vacancies, dislocations, and implanted Ar atoms) and the reordering of the surface Co spins due to the ion-beam bombardment, which act as pinning centers for domains during the magnetic reversal process. After the ion-beam bombardment with oxygen, the film's hysteresis loops maintained similar squareness (~0.8) with $H_c$ ranging from 4.32 kA/m to 8.36 kA/m. The field cooling to 180 K resulted in a reduced $H_c$ (2.39 kA/m to 5.97 kA/m) in the ion-beam bombarded samples. This is possibly due to the competition between the magnetocrystalline anisotropy of different phases. When the films were cooled to below the $T_N$ or $T_C$ of one (or more) phase, it (or they) starts to contribute to and gradually dominates the magnetization reversal processes of the films at low temperature. Squarer hysteresis loops ($M_r/M_{s.}$ ~ 0.9) was observed at 180 K, indicating an enhanced magnetic anisotropy at lower temperatures after field cooling [36]. Unlike the bilayers after in-situ bombardment where large $H_{ex}$ (~50 kA/m) was measured [30], only small loop shifts ($H_{ex}$ < 477 A/m) were observed in the hysteresis loops of all the post-bombarded samples. This is because Co was more readily oxidized into Co-oxide by in-situ oxidization, while relatively small amount of Co-oxide was formed after post bombardment, as inferred from the composition analyses above. This weak exchange coupling was unable to pin Co spins during magnetization reversal process. In order to further analyze the influence of oxygen content in the ion beam, the $H_c$ and $H_{ex}$ measured at 298 K and

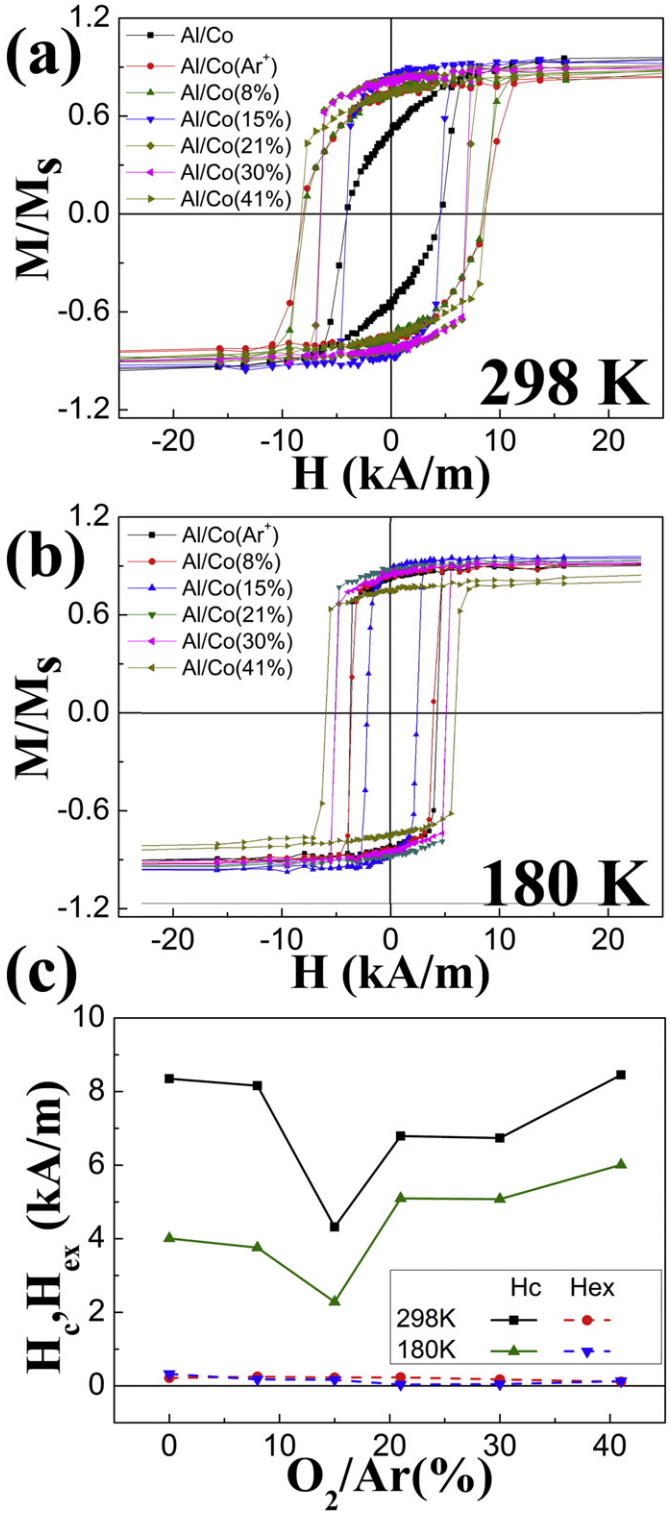


**Fig. 6.** Magnetic hysteresis loops measured at 298 K (a) and 180 K (b) after field cooling at 1.2 T magnetic field. (c) Magnetic coercivity ($H_c$) and exchange bias ($H_{ex}$) of Co bombarded by ion beam with $O_2$/Ar ratio ranging from 0 to 41% and capped with Al layer.

180 K were plotted against the $O_2$/Ar ratio, as shown in Fig. 6(c). Assuming $H_{ex}$(T) was similar between films (i.e. comparable blocking temperatures), at lower $O_2$/Ar ratios, $H_c$ decreases with increasing oxygen content. When the $O_2$/Ar ratio is higher than 15%, an enhanced $H_c$ was observed with the higher oxygen concentrations. Clearly, the ion-beam bombardment with oxygen plays an important role in Co anisotropy as well as magnetization reversal processes. Compared with the

un-bombarded films, the structural changes in the ion-beam bombarded Al/Co bilayers include the emergence of (1) bombardment-induced defects (vacancies, dislocations, and implanted ions), (2) diffused Al and O atoms in the grain boundaries, and (3) Co oxides. The first factor is considered to be to the same in all the ion-beam bombarded samples since the same $V_{EH}$ and Ar gas flow was used in the ion-beam bombardment. The diffused Al and O atoms inside the Co layer accumulate in the grain boundaries. Some Al atoms react with Co to form $CoAl_x$. With the increasing oxygen content in the ion beam, the concentration of the diffused Al increases, as shown in the XPS results. Similarly, it can be inferred that the content of the diffused O also increases with $O_2$/Ar ratio. These defects lead to lower $H_c$ since the diffused atoms and $CoAl_x$ reduce the overall magnetocrystalline anisotropy of the Co layers [37–39]. Besides, Co oxides were formed in the interfacial layer as a result of the ion-beam bombardment with oxygen. The Co oxides at domain walls acted as the pinning centers during the magnetization reversal, leading to the higher surface anisotropy, and the increased $H_c$. As the content of Co-oxides increases with the $O_2$/Ar ratio, this effect tends to increase $H_c$ at higher $O_2$/Ar ratio. This $H_c$ dependence on the $O_2$/Ar ratio is believed to be the result of competition between the reduction of magnetocrystalline anisotropy due to Al and O diffusion and the increase in surface anisotropy due to Co-oxide formation. At lower $O_2$/Ar ratio, the content of Co oxide is relatively low, so the pinning effect at the domain wall is also relatively weak over the whole film's magnetism. However, relatively high Al concentration in Co was characterized by XPS (10–20%). This indicates that the ion-beam bombardment effects on the overall magnetism were defect-induced reductions of the magnetocrystalline anisotropy. This resulted in the lowest $H_c$ (4.32 kA/m at 298 K) for the 15% $O_2$/Ar sample. The domain wall pinning effects of Co oxides are dramatically increased with increasing $O_2$/Ar ratio, while the concentration of diffused Al and O gradually approaches saturation. So the overall $H_c$ is dominated by the surface anisotropy enhancement induced by Co oxides at $O_2$/Ar higher than 15%. This mechanism leads to the increasing $H_c$ with $O_2$/Ar ratio until the highest $H_c$ (5.97 kA/m) at 41% $O_2$/Ar.

The temperature dependence of the low field (10 mT) magnetization from ZFC and FC processes are presented in Fig. 7. In all the films, the magnetization decreased monotonically with increasing temperature. FC and ZFC curves exhibited only small variations in most of the samples due to the similar crystallite sizes (resulting in similar onset temperatures of superparamagnetism, which are above 300 K since $H_c$'s are still measurable at that temperature) and the high Curié temperature of Co ($T_C$ ~ 1388 K [7]). However, the separated FC and ZFC curves merge at around 320 K, which is known as the irreversibility temperature ($T_{irr}$). This is likely due to the magnetic transition of CoO from AF to paramagnetic above $T_N$ ~ 291 K. The uncompensated AF interfacial spins begin to give rise to enhanced moment at lower temperatures [40,41]. The smaller content of CoO in this experiment is also responsible for the little difference in the FC and ZFC curved in Fig. 7. Further characterization down to 5 K to obtain blocking temp or significant separation between FC and ZFC is in progress.

## 4. Conclusions

The influence of oxygen content used during the post-deposition ion-beam bombardment on Co layers' magnetism was investigated in this paper. Different microstructure and magnetic properties were observed compared with the in-situ treatment reported previously. Naturally oxidized $Al_2O_3$, B2 CoAl, and HCP Co existed in the unbombarded Al capped Co film. Increasing the oxygen content in the ion beam resulted in the formation of amorphous $Al_2O_3$, rock-salt CoO, and spinel $Co_3O_4$ in the Al/Co interface. The magnetic properties of the Co film were also modified due to these compositional and microstructural changes. The $Ar^+$ ion-beam bombardment created defects in Co layer and resulted in pinned Co interface spins, resulting in enhanced anisotropy and higher $H_c$ (from 4.14 kA/m to 7.96 kA/m). Both enhanced and reduced $H_c$ were observed after the ion-beam bombardment with oxygen due to the competing effects between the reduced magnetocrystalline anisotropy by Al and O diffusion (which decreased $H_c$) and the increased surface anisotropy by the pinning effect of Co oxides at domain walls (which increased $H_c$).The low field magnetization (susceptibility) increased monotonically with decreasing temperature during ZFC and FC measurements, with an irreversibility temperature at around 320 K in the Al/Co–O (21% $O_2$/Ar)/Co. This work provides an effective method for the modification of the structural, compositional,

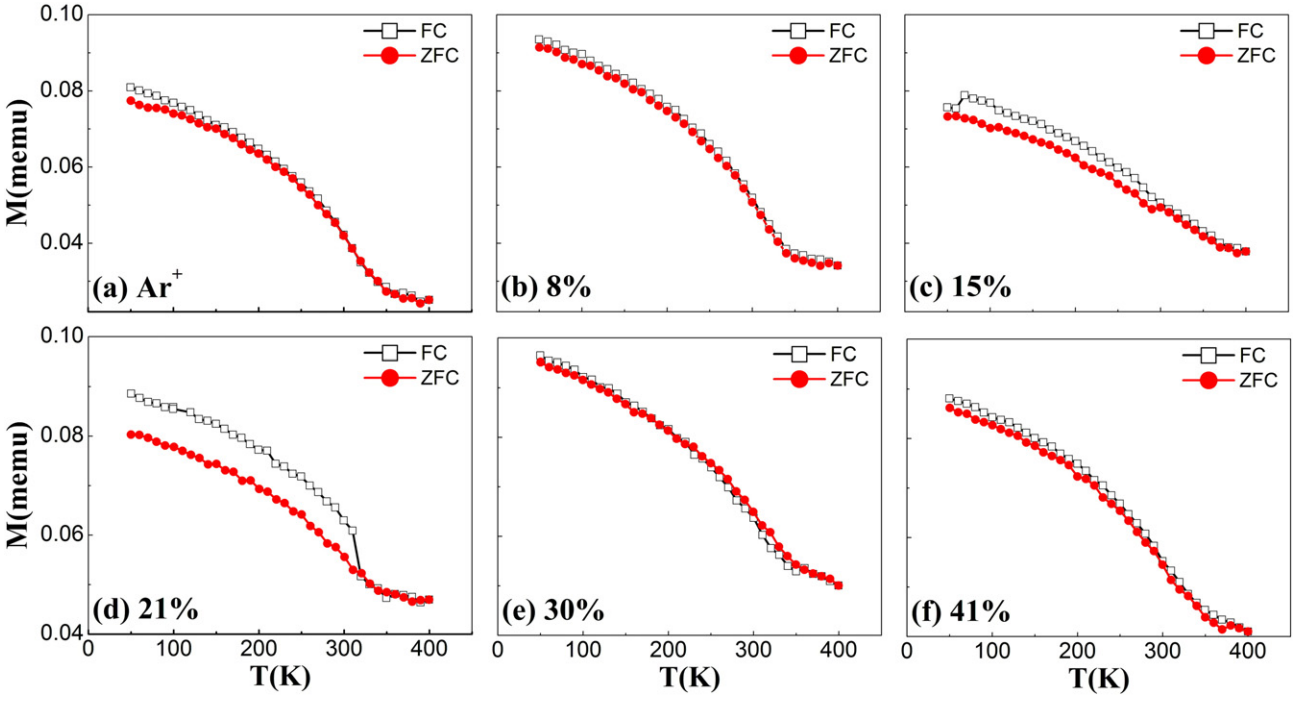


**Fig. 7.** Temperature dependence of magnetic moment of ion-beam bombarded Co capped with Al layer after field cooling (FC) and zero field cooling (ZFC) process.

and magnetic properties of Co layers through ion-beam bombardment with oxygen and argon.

## Acknowledgments

This work was supported by the Seed Funding for Basic Research and Small Project Funding from the University of Hong Kong, the RGC-GRF grant (HKU 704911P), ITF Tier 3 Fundings (ITS/104/13, ITS/112/12), the University Grants Committee of Hong Kong (contract no. AoE/P-04/08), the Natural Sciences and Engineering Research Council (NSERC) of Canada, the Ministry of Science and Technology (MOST) of Taiwan, and the Norwegian Research Council.

## References

[1] S.M. Thompson, J. Phys. D. Appl. Phys. 41 (2008) 093001.
[2] I.L. Prejbeanu, S. Bandiera, J. Alvarez-Hérault, R.C. Sousa, B. Dieny, J.P. Nozières, J. Phys. D. Appl. Phys. 46 (2013) 074002.
[3] K.W. Lin, M. Mirza, C. Shueh, H.R. Huang, H.F. Hsu, J. van Lierop, Appl. Phys. Lett. 100 (2012) 122409.
[4] X. Li, K.W. Lin, H.Y. Liu, D.H. Wei, G.J. Li, P.W.T. Pong, Thin Solid Films 570 (2014) 383.
[5] J. Nogués, I.K. Schuller, J. Magn. Magn. Mater. 192 (1999) 203.
[6] P.A. Joy, P.S.A. Kumar, S.K. Date, J. Phys. Condens. Matter 10 (1998) 11049.
[7] P. Enghag, Encyclopedia of the Elements: Technical Data - History - Processing - Applications, John Wiley & Sons, 2008.
[8] P. Gambardella, S. Rusponi, M. Veronese, S.S. Dhesi, C. Grazioli, A. Dallmeyer, I. Cabria, R. Zeller, P.H. Dederichs, K. Kern, C. Carbone, H. Brune, Science 300 (2003) 1130.
[9] V.A. de la Peña O'Shea, I.d.P.R. Moreira, A. Roldán, F. Illas, J. Chem. Phys. 133 (2010).
[10] P.Y. Yang, X.Y. Zhu, G. Chen, F. Zeng, F. Pan, J. Appl. Phys. 107 (2010).
[11] R. Sbiaa, H. Meng, S.N. Piramanayagam, Phys. Status Solidi 5 (2011) 413.
[12] P.S. Silinsky, M.S. Seehra, Phys. Rev. B 24 (1981) 419.
[13] W.L. Roth, J. Phys. Chem. Solids 25 (1964) 1.
[14] W.H. Meiklejohn, C.P. Bean, Phys. Rev. 105 (1957) 904.
[15] F. Radu, M. Etzkorn, R. Siebrecht, T. Schmitte, K. Westerholt, H. Zabel, Phys. Rev. B 67 (2003) 134409.
[16] F. Radu, M. Etzkorn, T. Schmitte, R. Siebrecht, A. Schreyer, K. Westerholt, H. Zabel, J. Magn. Magn. Mater. 240 (2002) 251.
[17] S. Laureti, S.Y. Suck, H. Haas, E. Prestat, O. Bourgeois, D. Givord, Phys. Rev. Lett. 108 (2012) 077205.
[18] M. Gierlings, M.J. Prandolini, H. Fritzsche, M. Gruyters, D. Riegel, Phys. Rev. B 65 (2002) 092407.
[19] M.R. Ghadimi, B. Beschoten, G. Güntherodt, Appl. Phys. Lett. 87 (2005).
[20] M. Gruyters, J. Appl. Phys. 95 (2004) 2587.
[21] J.B. Yi, J. Ding, J. Magn. Magn. Mater. 303 (2006) e160–e164.
[22] S. Laureti, E. Agostinelli, G. Scavia, G. Varvaro, V.R. Albertini, A. Generosi, B. Paci, A. Mezzi, S. Kaciulis, Appl. Surf. Sci. 254 (2008) 5111.
[23] J. Demeter, E. Menéndez, A. Teichert, R. Steitz, D. Paramanik, C. Van Haesendonck, A. Vantomme, K. Temst, Solid State Commun. 152 (2012) 292.
[24] J. Demeter, E. Menéndez, A. Schrauwen, A. Teichert, R. Steitz, S. Vandezande, A.R. Wildes, W. Vandervorst, K. Temst, A. Vantomme, J. Phys. D. Appl. Phys. 45 (2012) 405004.
[25] C. David Laurence, S. Chin, C. Pei-shi, G. Jian-Fa, K. Frank, L. Jan van, L. Ko-Wei, Jpn. J. Appl. Phys. 51 (2012) 11PG01.
[26] W. Peiwen, P. Liangqiang, T. Xinlin, W. Xiaogong, Y. Jun, Nanotechnology 16 (2005) 1693.
[27] V. Nefedov, D. Gati, B. Dzhurinskii, N. Sergushin, Y.V. Salyn, Zh. Neorg. Khimii 20 (1975) 2307.
[28] V.V. Nemoshalenko, V.V. Didyk, V.P. Krivitskii, A.I. Senekevich, Zh. Neorg. Khimii 28 (1983) 2182.
[29] G. Tyuliev, S. Angelov, Appl. Surf. Sci. 32 (1988) 381.
[30] D. Cortie, C. Shueh, P.-S. Chen, J.-F. Gao, F. Klose, J. van Lierop, K.-W. Lin, Jpn. J. Appl. Phys. 51 (2012) 11PG01.
[31] M. Segall, P.J. Lindan, M.A. Probert, C. Pickard, P. Hasnip, S. Clark, M. Payne, J. Phys. Condens. Matter 14 (2002) 2717.
[32] J.P. Perdew, W. Yue, Phys. Rev. B 33 (1986) 8800.
[33] J.P. Perdew, J. Chevary, S. Vosko, K.A. Jackson, M.R. Pederson, D. Singh, C. Fiolhais, Phys. Rev. B 46 (1992) 6671.
[34] D.R. Lide, CRC Handbook of Chemistry and Physics, CRC press, 2004.
[35] T.J. Konno, S. Yamamuro, K. Sumiyama, J. Appl. Phys. 90 (2001) 3079.
[36] T. Ambrose, C.L. Chien, J. Appl. Phys. 83 (1998) 7222.
[37] C. Abraham, A. Aharoni, Phys. Rev. 120 (1960) 1576.
[38] Y. Khan, Phys. Status Solidi A 23 (1974) K151–K154.
[39] W.Y. Zhang, X.Z. Li, S. Valloppilly, R. Skomski, D.J. Sellmyer, Mater. Sci. Eng. B 186 (2014) 64.
[40] J. van Lierop, B.W. Southern, K.W. Lin, Z.Y. Guo, C.L. Harland, R.A. Rosenberg, J.W. Freeland, Phys. Rev. B 76 (2007) 224432.
[41] J. van Lierop, K.W. Lin, J.Y. Guo, H. Ouyang, B.W. Southern, Phys. Rev. B 75 (2007) 134409.